Near-field wave-function spectroscopy of excitons and biexcitons

Erich Runge*

Technische Universität Ilmenau, Fachgebiet Theoretische Physik I, Postfach 100565, 98684 Ilmenau, Germany

Christoph Lienau†

Max-Born-Institut für Nichtlineare Optik und Kurzzeitspektroskopie, Max-Born-Straße 2A, 12489 Berlin, Germany

Improvements in spatial resolution of near-field spectroscopy have recently allowed for wave-function imaging of single excitons and biexcitons localized in semiconductor quantum wells. Surprisingly, the apparent extent of the biexciton wave function was found to be considerably reduced compared to a single exciton. We analyze theoretically the image contrast in general near-field wave-function mapping, taking into account the finite spatial resolution of the experiment. In particular, we show that due to the nonlinear nature of biexciton spectroscopy, a smaller biexciton image size is expected even if the spatial resolution is insufficient to resolve the wave functions.

During recent years, the spatial resolution of low-temperature near-field (NSOM) spectroscopy has been improved considerably and now reaches down to about 20 nm.[1,2] This opens up a new route to locally study and possibly manipulate quantum phenomena in metallic, semiconducting, and organic nanostructures: It allows one to go beyond recording emission and/or absorption spectra of single nanostructures towards real-space imaging of wave functions of single quantum objects in nanostructures and devices.[3,4] In Ref. 3, the photoluminescence (PL) of single excitons (X) and biexcitons (XX) localized in interface thickness fluctuations [interface quantum dots (IQD)] of a thin GaAs quantum well (QW) was imaged with a resolution of about 30 nm. This is well below the apparent size of the measured X (100 nm) and XX (70 nm) PL images. Based on a theoretical model assuming infinitely high resolution, the images were related to the different extent of the X and XX center-of-mass (COM) wave functions.

In this paper, we theoretically analyze the image contrast in optical near-field wave-function spectroscopy, taking the finite spatial resolution explicitly into account. We investigate both weakly and strongly confining quantum dots and and identify several effects that influence the apparent size of exciton and biexciton wave function images. In order of decreasing importance we distinguish the following: (i) *NSOM mode*: Distinctly different excitation power dependencies in collection and illumination/collection geometries lead to variations in spatial image size. (ii) *Biexciton nonlinearity*: Biexciton generation and luminescence are intrinsically nonlinear processes and this again affects the spatial PL profile. Both effects give rise to pronounced reductions in XX versus X images size and, in particular, to a much smaller apparent XX size even if the spatial resolution is insufficient to resolve the wave functions. (iii) *Mass effects*: Depending on the spatial shape of the confinement potential, the heavier XX mass may lead to a reduction of the XX COM wave function by up to a factor of $1/\sqrt{2}$. (iv) *Optical resolution*: The finite aperture size of the near-field tip and electromagnetic propagation within the cap layer leads to a similar broadening ($\simeq 30$ nm) of the X and XX image size and, for narrow apertures, to anisotropic images. (v) The finite extent of the ex-

citon *relative wave function* has two opposing effects. Both are usually small [of the order of the average electron-hole distance $\ell_{eh} \lesssim 10$ nm (Refs. 5 and 6). On the one hand, the positions of the recombining electron-hole pair and the biexciton's COM are in general different. This widens the PL profile of the XX, but not the X. On the other hand, the COM of an extended object can approach a confining potential barrier only up to half its size. This reduces the size of the COM wave function more for the XX than for the X.[8] In the limit of very strong lateral confinement, both effects cancel each other exactly.

Our results indicate that a quantitative reconstruction of excitonic wave functions requires us to include at least the effects (i)–(iii) in the interpretation of near-field optical images. Depending on circumstances, (iv) and (v) can be relevant as well.

In shallow semiconductor quantum wells, excitons are localized due to unavoidable nanoscale fluctuations of the interface. Yet the interface quality of today's samples is so high that the extent of the exciton wave function in these IQDs is much larger than the X Bohr radius a_B. Thus, the optically active exciton wave function is rather well represented by a factorization[6]

$$\Psi_X^{\text{IQD}}(\vec{r}_e, \vec{r}_h) \approx \psi_X(\mathbf{R}_X) \cdot \varphi_X(\mathbf{r}_e - \mathbf{r}_h, z_e, z_h) \qquad (1)$$

into a center-of-mass wave function ψ_X depending on the in-plane COM position $\mathbf{R}_X$ and a part φ_X which comprises both the relative motion and the confinement in growth direction z, $[\vec{r}=(\mathbf{r},z)]$. A typical size of ψ_X is $25-100$ nm,[6] whereas the relative wave function extends over $a_B \simeq 7-10$ nm.[5,6] This large coherence of the exciton COM wave function results in extremely large excitonic dipole moments of $50-100D$,[9] and this strong coupling to light was directly confirmed in recent experiments.[10,11] In the calculations described below, we can thus use a standard effective-mass description and omit the cell-periodic Bloch factor.

About biexciton wave functions in IQD, much less is experimentally and theoretically known than about single-exciton wave functions. State-of-the-art calculations of wave functions in quantum wells indicate, in some similarity with

the hydrogen molecule, that the electron and hole of each exciton are strongly correlated and the center-of-mass positions are separated by roughly one Bohr radius.[12] For biexcitons bound to interface defects in shallow quantum wells,[13] the extent of the total biexciton wave function seems to be even smaller, only 10–25 % larger than the exciton extent. Therefore, in the large interface quantum dots considered here, the factorization of the biexciton wave function into a COM part ψ_{XX} depending on the biexciton in-plane position $\mathbf{R}_{XX}$ and a relative part φ_{XX} seems justified,[13]

$$\Psi_{XX}^{\mathrm{IQD}}(\vec{r}_{e1},\vec{r}_{e2},\vec{r}_{h1},\vec{r}_{h2}) \approx \psi_{XX}(\mathbf{R}_{XX})\varphi_{XX}$$
$$\times(\mathbf{r}_{e1}-\mathbf{r}_{hh},\mathbf{r}_{e2}-\mathbf{r}_{hh},\mathbf{r}_{h1}-\mathbf{r}_{h2},z_{e1},z_{e2},z_{h1},z_{h2}), \quad (2)$$

even though the limits of this approximation have not yet been analyzed in great detail. The arguments leading to the factorization in Eq. (1) for the exciton have been reviewed in detail in Ref. 6. They apply to the biexciton case as well. We choose a representation using the hole COM $\mathbf{r}_{hh}=(\mathbf{r}_{h1}+\mathbf{r}_{h2})/2$. For simplicity, we ignore the spin degrees of freedom and assume that the antisymmetry required by the Pauli principle is provided by the spin wave function. This is the case for the lowest optically active biexciton state. In a disorder-free QW, accurate relative wave functions φ_{XX} have been recently reported.[12] Here, average e-e and h-h separations are of the order of a_B, i.e., comparable to typical e-h distances[12] and the total extent of φ_{XX} is less than about $2a_B$ even for XX binding energies of only $\simeq 0.2$ meV. Thus, the extent of φ_{XX} is only slightly larger than that of a typical QW exciton. In IQD in thin QWs, XX binding energies of 1–3 meV are typically found,[14,15] and correspondingly the extent of φ_{XX} is expected to be even smaller.[13] Using the state-of-the-art wave functions,[12] the effective confinement potentials for the X and XX COM wave functions,[16] generated by convoluting the local disorder potential with $\varphi_{X,XX}$,[17] are nearly identical. Thus, the difference in extent of φ_X and φ_{XX} has only a small effect on the spatial extent of the X and XX COM wave functions. This is in contrast to predictions in Ref. 8 which suggest a different size of the relative wave functions as the most important ingredient in the interpretation of Ref. 3. This possibly results from the use of the simple variational XX wave function of Kleinman[18] in combination with the unrealistic assumption of square-well confinement and an uncritical application of arguments put forward by one of the present authors in Ref. 16.

We give analytical results for X and XX COM wave functions for two special cases of in-plane confinement: (a) by a smooth harmonic potential and (b) in a cylindrical box with infinitely high barriers. The corresponding COM wave functions are oscillator eigenfunctions and two-dimensional "spherical" waves,

$$(a): \psi_X(\mathbf{R}) = \frac{e^{-R^2/2\ell_0^2}}{\ell_0\sqrt{\pi}}, \quad \psi_{XX}(\mathbf{R}) = \frac{e^{-R^2/\ell_0^2}}{\ell_0\sqrt{\pi/2}}, \quad (3)$$

$$(b): \psi_X(\mathbf{R}) = \psi_{XX}(\mathbf{R}) = \frac{J_0(\kappa_0 R/\ell_{\mathrm{box}})}{\sqrt{\pi}\ell_{\mathrm{box}}J_1(\kappa_0)}, \quad (4)$$

with $\kappa_0 = 2.405$ being the first zero of the Bessel function J_0. The extensions ℓ_0 and ℓ_{box} are related to the full width at half

maximum ℓ_F of the exciton densities $|\psi_X(\mathbf{R})|^2$ via $\ell_0 = 1.665\ell_F$ and $\ell_{\mathrm{box}}=1.068\ell_F$.

For harmonic confinement, Eq. (3), ψ_{XX} is narrower by a factor of $1/\sqrt{2}$ than ψ_X due to the combined effect of the heavier mass $2m_X$ and the stronger confinement $V_c^{XX}\simeq 2V_c^X$. Both effects contribute for general confining potentials, but not for the cylindrical particle-in-a-box case (4), where both COM functions coincide. The latter is therefore an interesting limit for comparison.

A different picture emerges in strongly confined dots, e.g., in Stranski-Krastanov quantum dots (SQDs), case (c). In lowest order, each electron or hole is confined on a single-particle level.

This is the case for both the $1e$-$1h$ states (termed X) and for the $2e$-$2h$ states (XX),

$$\Psi_X^{\mathrm{SQD}} \approx \phi(\vec{r}_e)\phi_h(\vec{r}_h), \quad (5)$$

$$\Psi_{XX}^{\mathrm{SQD}} \approx \phi_e(\vec{r}_{e1})\phi_e(\vec{r}_{e2})\phi_h(\vec{r}_{h1})\phi_h(\vec{r}_{h2}). \quad (6)$$

Particle-particle interactions can be accounted for perturbatively, in analogy to their treatment in atomic physics. A typical extent of Ψ_X^{SQD} is on the order of 10 nm, i.e., it is too small to be resolved with the current techniques.

Apart from the size of ψ_X and ψ_{XX}, another important length scale in near-field wave-function imaging is introduced by the lateral dimension of the electromagnetic field in the quantum-well plane. For many purposes, the field structure inside the near-field aperture and field propagation through the semiconductor material are well approximated by the Bethe-Bouwkamp model.[19] It describes the electromagnetic field below a circular aperture of radius a_0 in a perfectly conducting metal film illuminated with a plane wave linearly polarized along the x axis. The different boundary conditions for the normal and tangential components of the electric field give rise to a pronounced spatial anisotropy of the field directly below the aperture. While the x component of the field shows a divergence at the rim of the aperture, the maximum of the y component, perpendicular to the incident field polarization, lies in the center of the aperture (see, e.g., Fig. 11 in Ref. 20 and Ref. 19). This predicted spatial anisotropy could be confirmed in different experiments.[21,22] With increasing distance from the aperture,
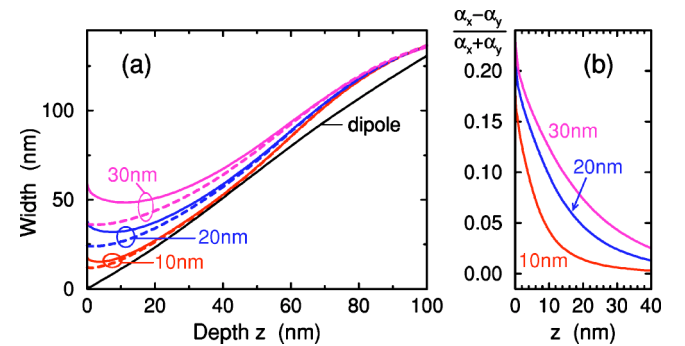

FIG. 1. (Color online) (a) Widths $2\sqrt{2\ln(2)}\alpha_{x,y}$ [x (y): solid (dashed) line] and (b) anisotropy of the electromagnetic field at depth z in a semiconductor with $n=3.5$ below circular apertures having different radii α_0. Thin line: point-dipole limit (isotropic).

centered at $\mathbf{R}_T(x_T, y_T)$, the evanescent, high-spatial-frequency components that give rise to the divergence at the rim decay more and more. At distances z of a few nm, the transverse field components are close to an elliptical field profile polarized parallel to the incident field. For even larger distances, $z > \lambda/(2\pi n)$, with n being the refractive index, the evanescent field components have decayed and now the spatial field distribution is well described by that of a magnetic point dipole.[19] The small longitudinal components of the transmitted field can safely be neglected since they are reduced by a factor of $1/n^2$ ($n \approx 3.5$ for GaAs) at the air/semiconductor interface and since heavy-hole excitons have only in-plane dipole moments.[6]

We characterize the depth dependence of the electromagnetic field profile by its second moments $\alpha_{x,y}$ along the principal axes. Results for various aperture radii are given in Fig. 1(a). It is important to notice that the boundary conditions at the rim of the aperture induce a rather pronounced anisotropy $r = (\alpha_x - \alpha_y)/(\alpha_x + \alpha_y)$ [Fig. 1(b)] for distances of up to $\simeq a_0$ even in the absence of an anisotropic medium. This electromagnetic anisotropy with field singularity in the aperture plane is particularly relevant in the regime of ultra high resolution with an aperture opening much smaller than the optical wavelength. This regime was hithertho experimentally not accessible and therefore has not been considered appropriately in theoretical semiconductor optics.

To calculate optical matrix elements, we invoke the usual approximation that the dipole operator $\sim i\hbar\vec{\nabla}$ acts only on the cell-periodic Bloch factor and explicitly use the factorized form of Eqs. (1) and (2). In near-field spectroscopy, the non-local response of the medium has to be taken into account.[23] The resulting transition amplitudes for $X \leftrightarrow$ photon and for $X +$ photon $\leftrightarrow XX$ with the near-field tip at position R_T are proportional to[6,7]

$$\mathcal{M} = C^{\text{IQD}} \int d\mathbf{R}\, \psi_i(\mathbf{R}) \mathcal{E}(\mathbf{R} - \mathbf{R}_T) \psi_f(\mathbf{R}), \qquad (7)$$

with states $\psi_i = 1$, $\psi_f = \psi_X$, and $\psi_i = \psi_X$, $\psi_f = \psi_{XX}$ for the X and XX transition, respectively. In optical transitions, the electron and hole are generated (annihilated) at the same spatial position [$\vec{r}_e = \vec{r}_h$ in Eq. (1) or Eq. (2)]. For the $X \leftrightarrow XX$ transition, this generation (annihilation) occurs in the presence of another e-h pair in the same QD. The currently investigated optically active quantum dot heterostructures are mostly buried by at least 20 nm below the sample in order to avoid nonradiative recombination processes. Therefore, the electric field profile within the quantum dot plane extends over at least 20 nm [Fig. 1(a)], even if an ideal pointlike dipole source was used. Therefore, the variation of the electric field is weak on the scale of the internal relative wave function of less than 10 nm.[6,12] This indicates that the integrations over the relative wave functions do not depend much on the electromagnetic field distribution and can be compounded into the factors C_X^{IQD} and C_{XX}^{IQD} together with Kane's matrix element and other constant prefactors.

Based on these considerations, we now discuss the contrast mechanism in near-field wave-function imaging. First, we assume that the experiment is performed in the illumination/collection (i-c) mode, i.e., the sample is locally excited through a near-field probe positioned at $\mathbf{R}_T$ and the emitted PL is collected through the same probe. In the case of resonant excitation, the detected PL signal is

$$\text{illum-collect: } I_X^{\text{i-c}}(\mathbf{R}_T) = |\mathcal{M}_X(\mathbf{R}_T)|^4. \qquad (8)$$

The nonlinearity arises because the probabilities for both exciton generation and detection scale as $|\mathcal{M}_X(\mathbf{R}_T)|^2$.

For nonresonant ("hot") excitation, the spatial variation of the generation probability evidently depends on the transport properties of the optically generated exciton population. Assuming a diffusion length that is much larger than the aperture size, the generation probability is almost independent of $\mathbf{R}_T$. As in the case of collection (c) mode experiments, the PL signal scales as

$$\text{collection mode: } I_X^{\text{c}}(\mathbf{R}_T) = |\mathcal{M}_X(\mathbf{R}_T)|^2. \qquad (9)$$

However, in the limit of negligible exciton transport, a good assumption for disordered QWs at low temperatures,[24] Eq. (8) holds again.

Similar arguments apply for the biexciton images, but now the generation probability in the i-c mode is proportional to the square of the local intensity,[14] i.e.,

$$I_{XX}^{\text{i-c}}(\mathbf{R}_T) = |\mathcal{M}_{XX}(\mathbf{R}_T)|^4 |\mathcal{M}_X(\mathbf{R}_T)|^2, \qquad (10)$$

$$I_{XX}^{\text{c}}(\mathbf{R}_T) = |\mathcal{M}_{XX}(\mathbf{R}_T)|^2. \qquad (11)$$

This nonlinear intensity dependence of the XX generation can give rise to important differences in the spatial variation of exciton and biexciton PL images, as will be discussed next. For the case of harmonic confinement and within the approximation of an elliptical field profile characterized by $\alpha_{x,y}$, Eqs. (8)–(11) can be evaluated analytically yielding elliptical PL profiles of Gaussian shape $I \sim \exp[-(x/\sigma_x)^2/2 - (y/\sigma_y)^2/2]$. Both the widths $\sigma_{x,y}$ and anisotropies r are clearly different for X and XX images. They are related to each other and to the ratio $\tilde{\alpha}_{x,y} = \alpha_{x,y}/\ell_0$ by (dropping x, y indices)

$$\text{IQD:}\, \sigma_X^{\text{i-c}} : \sigma_{XX}^{\text{i-c}} : \sigma_X^{\text{c}} : \sigma_{XX}^{\text{c}} : \ell_0$$

$$= \frac{\sqrt{1+\tilde{\alpha}^2}}{2} : \sqrt{\frac{1+4\tilde{\alpha}^2+3\tilde{\alpha}^4}{14+18\tilde{\alpha}^2}} : \sqrt{\frac{1+\tilde{\alpha}^2}{2}} : \sqrt{\frac{1+3\tilde{\alpha}^2}{6}} : 1$$

$$\xrightarrow{\tilde{\alpha}\to 0} 0.50 : 0.27 : 0.71 : 0.41 : 1.$$

These results are visualized in Fig. 2(a), for a fully numerical evaluation of Eq. (7) within the Bethe-Bouwkamp model.[19] It is seen that even for a perfect near-field probe, i.e., $\alpha \to 0$, a direct imaging of the X and XX wave function is possible neither in the c mode nor the i-c mode. In general, the reduction in size of XX images results not only from the change in mass and confinement potential but from a rather complex interplay between nonlinearity of the imaging process, spatial resolution, and wave-function size. This is clearly seen for the case of a cylindrical box [Fig. 2(b)]. Here, the extensions of X and XX wave functions are identical, yet a clear reduction of the size of the XX image is observed. It is less pronounced than for harmonic confine-
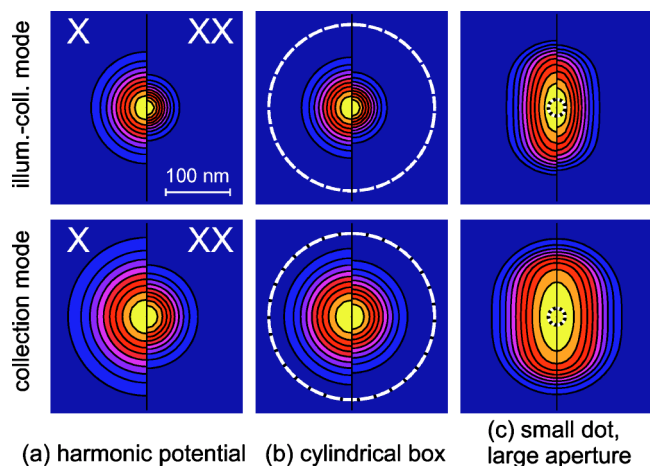
FIG. 2. (Color online) Calculated near-field images of excitons and biexcitons (left/right half-panels) in different quantum dots in GaAs ($n=3.5$) 20 nm below the surface for cases (a)–(c). In (a) and (b), $|\psi_X|^2$ has a FWHM of $\ell=100$ nm, much larger than the aperture radius $\alpha_0=10$ nm. In (c), $\alpha_0=80$ nm exceeds the X size: $\ell=10$ nm. PL intensity is color-coded in linear 10% steps. Dashed lines in (b) and (c) mark the cylindrical boxes.

ment because now only the nonlinearity effect contributes. Obviously, a rather good knowledge about the various experimental parameters is required to extract quantitative information from X and XX wave-function images. The situation is even more complex for very large QD where more than one X COM state will contribute to the XX optical matrix element (7).

The simplest, but maybe most surprising, case is that of $1e$-$1h$ and $2e$-$2h$ states in a very small quantum dot, case (c). Here, the luminescence profiles (8)–(11) are given by different powers of the field at the dot position, $I^{\mathrm{QD}} \sim |\mathbf{E}(\mathbf{R}_T)|^\nu$, leading to apparent widths

$$\text{SQD: } \sigma_X^{\mathrm{i\text{-}c}} : \sigma_{XX}^{\mathrm{i\text{-}c}} : \sigma_X^{\mathrm{c}} : \sigma_{XX}^{\mathrm{c}} : \alpha = \frac{1}{2} : \frac{1}{\sqrt{6}} : \frac{1}{\sqrt{2}} : \frac{1}{\sqrt{2}} : 1.$$

Obviously none of these profiles reflects the shape of the wave function, which is too small to be resolved. Yet, aniso-

tropic PL images are obtained and the apparent size of the XX image in the i-c mode is smaller than that of the X, see Fig. 2(c). Whereas the anisotropy reflects the anisotropic electromagnetic field within the QW layer [Fig. 1(b)], the reduction in size of the XX image results solely from the nonlinear nature of the experiment.

In summary, we have discussed the effects of a finite spatial resolution on the image contrast in near-field wave-function spectroscopy. We show that in general even for ideal near-field probes, a direct imaging of wave functions is possible only for excitons in a collection mode geometry. In all other cases (biexcitons, large aperture, or i-c mode) the PL contrast reflects a nontrivial interplay between nonlinear intensity dependence of the imaging process, spatial resolution, and wave-function size. Of special interest is the case of strongly confined quantum dots where none of the profiles reflects the shape of the wave function, but nevertheless anisotropic "images" are obtained with the XX image appearing smaller than the X image. Clearly, both spatial resolution and image formation play a major role in near-field wave-function spectroscopy.

We have introduced a simplified model in order to estimate semiquantitatively the relative importance of the different physical effects (i)–(v) on exciton and biexciton images. We expect that this model will prove useful in designing future experiments on metallic, semiconducting, and organic nanostructures. For a quantitative decription of particular experiments, one may have to go beyond our simplifying assumptions (weak lateral field variations, scalar representation of electromagnetic near fields,…). Computer codes allowing full vectorial solutions of Maxwell's equations for fixed dielectric configurations are readily available today. However, the inclusion of the resonant material response of the localized exciton states itself[7] remains a challenge.

*Electronic address: runge@tu-ilmenau.de

†Electronic address: lienau@mbi-berlin.de

[1] K. Matsuda, T. Saiki, S. Nomura, M. Mihara, and Y. Aoyagi, Appl. Phys. Lett. **81**, 2291 (2002).

[2] A. Hartschuh, E. J. Sanchez, X. S. Xie, and L. Novotny, Phys. Rev. Lett. **90**, 095503 (2003).

[3] K. Matsuda, T. Saiki, S. Nomura, M. Mihara, Y. Aoyagi, S. Nair, and T. Takagahara, Phys. Rev. Lett. **91**, 177401 (2003).

[4] Phys. Rev. Focus **12**, story 15 (2003); R. Fitzgerald, Phys. Today **56** (11), 14 (2003); Physik J. **5** (1), 17 (2004).

[5] D. Gammon, E. S. Snow, B. V. Shanabrook, D. S. Katzer, and D. Park, Phys. Rev. Lett. **76**, 3005 (1996).

[6] E. Runge, *Solid State Physics* (Academic Press, San Diego, 2002), Vol. 57, pp. 149–305, and references therein.

[7] V. Savona, *Disorder*, in *Electron and Photon Confinement in Semiconductor Nanostructures*, edited by B. Deveaud, A. Quattropani, and P. Schwendimann (IOS Press, Amsterdam, 2003), pp. 219–234.

[8] U. Hohenester, G. Goldoni, and E. Molinari, Appl. Phys. Lett. **84**, 3963 (2004).

[9] A. Thränhardt, C. Ell, G. Khitrova, and H. M. Gibbs, Phys. Rev. B **65**, 035327 (2002).

[10] J. R. Guest, T. H. Stievater, X. Ki, J. Cheng, D. G. Steel, D. S. Katzer, D. Park, C. Ell, A. Thränhardt, G. Khitrova, and H. M. Gibbs, Phys. Rev. B **65**, 241310 (2002).

[11] T. Guenther, C. Lienau, T. Elsaesser, M. Glanemann, V. M. Axt, T. Kuhn, S. Eshlaghi, and A. D. Wieck, Phys. Rev. Lett. **89**, 057401 (2002).

[12] C. Riva, F. M. Peeters, K. Varga, and V. A. Schweigert, Phys. Status Solidi B **234**, 50 (2002).

[13] O. Heller, Ph. Lelong, and G. Bastard, Phys. Rev. B **56**, 4702 (1997).

[14] K. Brunner, G. Abstreiter, G. Böhm, G. Tränkle, and G. Weimann, Phys. Rev. Lett. **73**, 1138 (1994).

[15] X. Li, Y. Wu, D. Steel, D. Gammon, T. H. Stievater, D. S. Katzer, D. Park, C. Piermarocchi, and L. J. Sham, Science **301**, 809 (2003).

[16] R. Zimmermann, F. Große, and E. Runge, Pure Appl. Chem. **69**, 1179 (1997).

[17] F. Intonti, V. Emiliani, C. Lienau, T. Elsaesser, V. Savona, E. Runge, R. Zimmermann, R. Nötzel, and K. H. Ploog, Phys. Rev. Lett. **87**, 076801 (2001).

[18] D. A. Kleinman, Phys. Rev. B **28**, 871 (1983).

[19] R. D. Grober, T. Rutherford, and T. D. Harris, Appl. Opt. **35**, 3488 (1996), and references therein.

[20] Y. Leviatan, J. Appl. Phys. **60**, 1577 (1986).

[21] E. Betzig and R. Chichester, Science **262**, 1422 (1993).

[22] J. A. Veerman, A. M. Otter, L. Kuipers, and N. F. van Hulst, Appl. Phys. Lett. **72**, 3115 (1998).

[23] O. Mauritz, G. Goldoni, F. Rossi, and E. Molinari, Phys. Rev. Lett. **82**, 847 (1999).

[24] V. Emiliani, F. Intonti, C. Lienau, T. Elsaesser, R. Nötzel, and K. H. Ploog, Phys. Rev. B **64**, 155316 (2001).